



Research Article

A Facile Synthesis of Montmorillonite Supported CdAl₂O₄ Nanocomposites with Photocatalytic and Hydrophobic Properties

KRISHNAN KALPANA¹, KUMAR RAJATHI²

¹ Thiruvalluvar University, Serkadu, Tamil Nadu, India

² Department of Chemistry, Kalaignar Karunanidhi Government Arts College, Tamil Nadu, India

Email: rajathi_sridhar@rediffmail.com

Citation: Kalpana, K., Rajathi, K. (2025) A Facile Synthesis of Montmorillonite Supported CdAl₂O₄ Nanocomposites with Photocatalytic and Hydrophobic Properties. *Substantia* 9(1): 23-31. doi: 10.36253/Substantia-2841

Received: Jul 04, 2024

Revised: Jan 16, 2025

Just Accepted Online: Jan 17, 2025

Published: Mar 5, 2025

Copyright: © 2025 Kalpana, K., Rajathi, K. This is an open access, peer-reviewed article published by Firenze University Press (<http://www.fupress.com/substantia>) and distributed under the terms of the Creative Commons Attribution License, which permits unrestricted use, distribution, and reproduction in any medium, provided the original author and source are credited.

Data Availability Statement: All relevant data are within the paper and its Supporting Information files.

Competing Interests: The Author(s) declare(s) no conflict of interest.

Abstract. The hydrothermal co-precipitation method was successfully employed to synthesize CdAl₂O₄ supported by natural clay, montmorillonite to reduce the toxicity of solid and liquid wastes that cause serious harm to livestock and humans due to the discharge of dye wastes into water bodies. Characterization of the montmorillonite/CdAl₂O₄ (MMT/CdAl₂O₄) composite was carried out using various techniques, including X-ray powder diffraction (XRD), scanning electron microscopy (SEM), high-resolution transmission electron microscopy (HR-TEM), photoluminescence spectroscopy (PL), diffuse reflectance spectroscopy (DRS), and BET surface area analysis. Experimental results indicate that CdAl₂O₄ supported by montmorillonite at a 9% wt concentration exhibited superior photocatalytic activity compared to undoped CdAl₂O₄ in the removal of the azo dye rhodamine-B (rh-B) under solar light irradiation. The FE-SEM images clearly reveal the formation of nanoclusters and nanoflakes interconnected via edge-to-flat-surface conjunction. Furthermore, BET analysis demonstrated that the surface area of MMT/CdAl₂O₄ surpasses that of undoped CdAl₂O₄. Remarkably, montmorillonite-supported CdAl₂O₄ exhibited excellent photocatalytic activity for up to four consecutive uses. A notable feature of montmorillonite/ CdAl₂O₄ is its high hydrophobicity, as evidenced by a contact angle of 113.8°. This hydrophobic nature is particularly advantageous in the production of self-cleaning materials.

Keywords: Montmorillonite clay; CdAl₂O₄ nanoflakes; Rhodamine-B; Photodegradation; Contact angle

1. INTRODUCTION

In recent decades, heterogeneous photocatalysis has gained recognition as an eco-friendly method for energy conversion. Semiconductor photocatalysts, in particular, have shown great promise for environmentally cleaning by facilitating the degradation of organic contaminants [1-3]. Semiconductor-mediated photocatalysis is one of the most successful methods available for cleaning and dye purification procedures. Metal oxide coupling has been proven to be an effective method to improve the photo-

catalytic activities of nanomaterials, which can reduce the recombination of the photogenerated electron/hole pairs and lengthen their lifetime [4,5]. A number of surface active materials such as activated carbon, zeolites, graphene and clay materials have been used as photocatalyst supports [6-8].

Natural clay materials, such as coal fly ash, bentonite, kaolinite, sepiolite, and montmorillonite, have demonstrated excellent support for semiconductor oxide materials in various photocatalytic studies [9-14]. Due to its softness, plasticity, porosity, tangibility, pliability, and climatic adaptability, all at affordable cost, were viable characteristics to recognize its usefulness, and introduced several products. Among the many kinds of clay minerals, montmorillonite has been recognized as an effective adsorbent due to its high surface area, expandability, and swellability, montmorillonite within the smectite group has been found to be an effective adsorbent for the removal of dyes and cations. The structure and cation exchange capacity (CEC) of montmorillonite are linked to its adsorption capability. Because of its structure, montmorillonite clay interacts with cations and accommodates them in the voids between layers, giving it the properties of a molecular sieve. In general, the mineral's net negative charge determines Montmorillonite's adsorption capacity. MMT can also be used as a coagulant in ponds when it is finely powdered. When added to water, it causes the water to become "clouded," draws in tiny particles, and eventually sinks to the bottom. Although MMT effectively absorbs heavy metals, its impact on human health is still unknown [16-20].

Spinel oxides, denoted by the formula AB_2O_4 with trivalent (B) and divalent (A) cations occupy octahedral and tetrahedral positions, while oxygen ions create a cubic unit cell. These materials are known for their chemical and thermal stability, finding applications in various fields like humidity sensors, ceramic catalysis, and magnetic materials [21]. Spinel compounds (general formula AB_2O_4) are part of a large family of inorganic materials and have become the subject of extensive research in numerous industrial processes, as well as in the realm of nanoscience and technology [22]. Their unique properties, such as high electrical resistivity, high coercivity, and moderate saturation magnetization, make them promising candidates for advanced applications in drug delivery systems, power electronics, sensors, catalysts, and spintronics [23-25]. Furthermore, aluminum spinel can be used as a suitable charge carrier and photocatalyst for a range of applications due to its exceptional optical, thermal, electrical, and magnetic properties. Cadmium aluminate ($CdAl_2O_4$) is a significant spi-

nel material and it has crucial applications in microwave devices, sensors, light helmets, light-emitting diodes, luminescence, pigment, gas sensors, and photocatalysts [26-29].

Rafiq et al. in their review assessed that, the ability of several nanomaterials to clean up dye-contaminated aquatic systems by focussing on essential parameters that affect the photocatalytic decolorisation of dyes. Numerous semiconductor nanocatalysts have demonstrated the ability to function as photocatalysts in the treatment of wastewater that contains textile colours. Operational characteristics are significantly impacted by photocatalyst efficiency. The nature of the sample to be degraded must be investigated because the impact of different parameters has occasionally proven contentious. Higher pH causes some reactive dyes to deteriorate, while lower pH causes others to do so. For photocatalytic dye degradation in wastewater, the reaction should therefore be conducted at the proper pH. The photocatalytic decolorisation of any dye is discovered to be influenced by a variety of factors, including reaction temperature, photocatalyst concentration, light intensity and irradiation duration, and dopant impact [30].

The co-precipitation technique has been widely used to prepare nanoparticles. It entails the simultaneous precipitation of multiple substances from a solution. With the help of a base and a solvent, metal hydroxides precipitate from salt precursors in an eco-friendly and economical manner. Co-precipitation is an easy method with controlled size distribution, high yield, and solvents that are safe for the environment for creating inorganic and metal-based nanoparticles. Given these advantages, we utilized co-precipitation techniques to prepare $CdAl_2O_4$. Herein, we successfully synthesized montmorillonite-supported $CdAl_2O_4$ and assessed its photocatalytic ability through the removal of rhodamine-B by solar-light radiation. Additionally, we investigated the hydrophobic nature of montmorillonite/ $CdAl_2O_4$.

2. MATERIALS AND METHODS

2.1 Chemicals and Reagents

$Al(NO_3)_3 \cdot 9H_2O$, $Cd(CH_3COO)_2 \cdot 2H_2O$, NaOH, EtOH and Montmorillonite clay ($(Na,Ca)_{0.3}(Al,Mg)_2Si_4O_{10}(OH)_2 \cdot nH_2O$) were supplied by Himedia chemicals, Rhodamine-B (Rh-B; $C_{28}H_{31}ClN_2O_3$; M.W- 479.01-CAS 81-88-9) dye was supplied by CDH (P) Limited. The purity of all the purchased chemicals were AR grade (99 % purity). Distilled water was used over the experiments.

2.2 Characterization Techniques

X-Ray diffraction (XRD) pattern of catalysts were obtained using a Siemens D5005 diffractometer with Cu K α ($\lambda = 0.151418$ nm) radiation. The diffractograms were recorded in 2θ range between 10 and 80° in steps of 0.02° with count time of 20s at each point. The morphology of catalyst was examined using Model ULTRA-55 field emission scanning electron microscope (FE-SEM). Samples were mounted on a gold platform placed in the scanning electron microscope for taking images at various magnifications. HR-TEM images were taken using the 200kV Ultra High Resolution Transmission Electron Microscope JEOL-2010, having high resolution Optical microscope and Leica microscope. A small quantity of catalyst suspension was dropped onto copper grids with holey carbon film. The grids were dried under natural conditions and examined. The diffuse reflectance spectra of all the catalysts were recorded in Shimadzu UV 2450 model equipped with an integrating sphere and using powdered BaSO₄ as a reference. The photoluminescence (PL) spectrum at room temperature was recorded using a Perkin-Elmer LS 55 fluorescence spectrometer. The specific surface areas of the catalysts were determined using a Micromeritics ASAP 2020 sorption analyzer. The samples were degassed at 423K for 12 hours and analysis was performed at 77K with N₂ gas as the adsorbate. The Brunauer-Emmett-Teller (BET) multipoint method least-square fit provided the specific surface area. The hydrophobicity of catalyst coating was obtained from the water contact angle. A drop shape analyser (DSA) (Kruss GmbH Germany) was used to record the contact angle.

2.3 Synthesis of montmorillonite supported CdAl₂O₄

The synthesis of both pure CdAl₂O₄ and MMT supported CdAl₂O₄ samples were carried out through a co-precipitation method. Initially, 50mL of 0.5M Al(NO₃)₃.9H₂O and 50mL of 0.3M Cd(CH₃COO)₂.2H₂O were separately dissolved in 50mL of distilled water. After that, the Cd(CH₃COO)₂.2H₂O solution was slowly added to Al(NO₃)₃.9H₂O solution with vigorous stirring. Subsequently, 0.500g (9% wt) of MMT powder, mixed with 10mL of ethanol, was introduced to the previous solutions with constant stirring. Following this, 0.2M of NaOH was dissolved in 30mL of distilled water followed by slowly adding to the combined aqueous solutions. The resulting solution was stirred at 80°C for 5 hours. The resulting product was collected by washing with ethanol and distilled water, and dried at 100°C for 5 hours. Finally, the MMT supported CdAl₂O₄ nanoparticles were

calculated for 6 hours at 700°C, denoted as 9% wt MMT/CdAl₂O₄ for easy understanding. The pure CdAl₂O₄ nanoparticles and 5% wt MMT supported CdAl₂O₄ were synthesized by the similar process for comparison.

2.4 Photocatalytic degradation

Photocatalytic degradation experiments were performed in summer days from 11 am to 2 pm under a direct sunlight illumination (Tiruvannamalai, Tamilnadu, India). A transparent borosilicate glass tube with 40 cm in height and 20mm in diameter was employed as reaction vessel. After 30 minutes of magnetic stirring in the dark, the dye and MMT/CdAl₂O₄ solutions reached equilibrium of adsorption and desorption. The photo-degradation process was carried out outdoors. To ensure thorough mixing of the reaction solution and to introduce oxygen, a pump was used to continuously aerate a 50mL dye solution containing MMT/CdAl₂O₄. There was no significant solvent evaporation during the lighting period. The first sample was collected during the adsorption phase while it was still dark. A two-milliliter sample was retained, and at predetermined intervals, it was centrifuged and diluted to ten milliliters. The solar light intensity, evaluated with the LT Lutron LX-10/A Digital Lux meter, was $I_{\text{solar}} = 1250 \times 100 \text{Lux} \pm 10$.

2.5 Contact angle measurements

Water contact angles were measured on a Drop Shape Analyzer (DSA) from Kruss GmbH in Germany. The volume of the water droplet was about 4 μ L based on at least four measurements. The average of these values represented the substrate's water contact angle (WCA). Spin coating was successfully applied to glass substrates to produce MMT/CdAl₂O₄-modified silane coatings at room temperature. MMT/CdAl₂O₄ photocatalyst-coated substrates were heated at 125°C for 2 hours in a controlled furnace to confirm the densification of the gel network.

3. RESULTS AND DISCUSSION

3.1 Characterization of nanocomposite

X-ray diffraction (XRD) measurement was conducted to assess the crystallinity of the synthesized photocatalysts. Figure 1a-c present the XRD patterns for undoped CdAl₂O₄, 5% wt MMT/CdAl₂O₄, and 9% wt MMT/CdAl₂O₄ photocatalysts. In Figure 1a,

the undoped $CdAl_2O_4$ photocatalyst displays the diffraction peaks at 13.75° , 19.25° , 26.37° , 31.02° , 33.56° , 37.50° , 38.85° , 55.18° , and 67.60° , which were corresponding to the (012), (300), (131), (042), (241), (431), (223), (520), and (713) planes of monoclinic primitive $CdAl_2O_4$ (JCPDS No. 34-0071). [31, 32]. Fig. 1b represents the diffraction peaks of montmorillonite clay alone. Meanwhile, in Figure 1c and 1d, newly formed peaks indicated by star symbols corresponded well with raw MMT for SiO_2 , Fe_2O_3 , MgO and Al_2O_3 , confirming the presence of MMT clay in the $MMT/CdAl_2O_4$ photocatalysts [33].

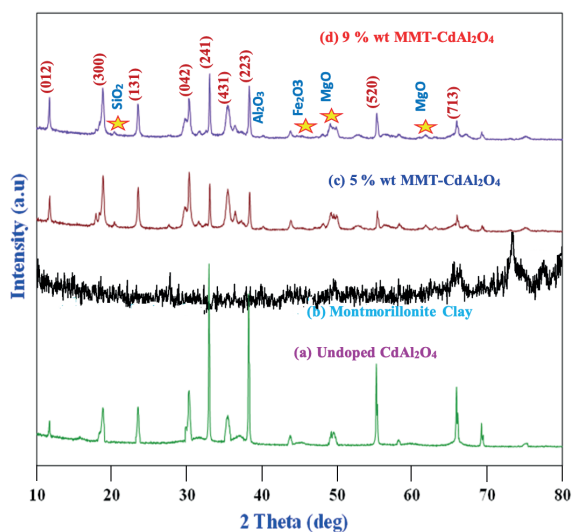


Fig. 1 XRD patterns of the (a) undoped $CdAl_2O_4$ (b) Montmorillonite clay (c) 5% wt $MMT/CdAl_2O_4$ and (d) 9% wt $MMT/CdAl_2O_4$ photocatalysts

A typical diffraction peak of montmorillonite clay is observed around 7.25° corresponding to basal spacing of 13.46\AA (Fig. SI 1). And after intercalation of $CdAl_2O_4$ this peak disappears. Importantly, no crystalline impurities or typical diffraction peaks were observed, indicating the good purity of the synthesized photocatalysts. Furthermore, the Scherrer equation was utilized to calculate the crystallite sizes of $CdAl_2O_4$.

$$\Phi = \frac{K\lambda}{\beta \cos\theta} \quad (1)$$

In this equation, Φ , λ , K , β and θ represents the crystalline size, the wavelength of the X-ray used, the shape factor, the full line width at the half-maximum height of the peak, and the Bragg angle, respectively.

Using this equation, the average crystallite size of hexagonal $CdAl_2O_4$ was determined to be 36.8 nm .

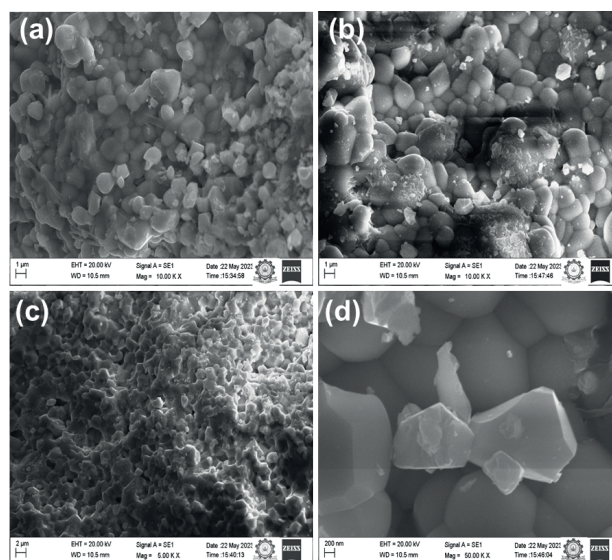


Fig. 2 FE-SEM images of the 9% wt $MMT/CdAl_2O_4$ photocatalyst at various magnifications: (a, b) $1\ \mu\text{m}$ (c) $2\ \mu\text{m}$ and (d) 200 nm

The surface structure and particle sizes of the synthesized samples were investigated using scanning electron microscopy (SEM) and high-resolution transmission electron microscopy (HR-TEM) techniques. SEM images of the 9% wt $MMT/CdAl_2O_4$ photocatalyst are presented in Figure 2a-d, revealing a flake-like morphology with intermittent nanosponge like particle. The presence of MMT particles is likely responsible for the observed surface morphologies. The elements present in the montmorillonite clay were confirmed by EDAX image (Fig. SI 3). The microstructures exhibit a nanosponge-like structure with high porosity. Micro-size hierarchical shape composed of nano-sized building blocks offer several advantages, including numerous mesopores that enhance the transfer of organic materials.

Moreover, Figure 3a-d displays HR-TEM images of 9% wt $MMT/CdAl_2O_4$ photocatalyst, showing spherical and hexagonal particle shapes with uniform element distribution. The dark areas in the images indicate the presence of MMT clay on the surface of $CdAl_2O_4$. From the lattice fringes (Figure 3c), the d spacing value calculated as 0.214 nm . The selected area electron diffraction (SAED) image in (Figure 3d) confirms the occurrence of (131) plane of $CdAl_2O_4$ structure.

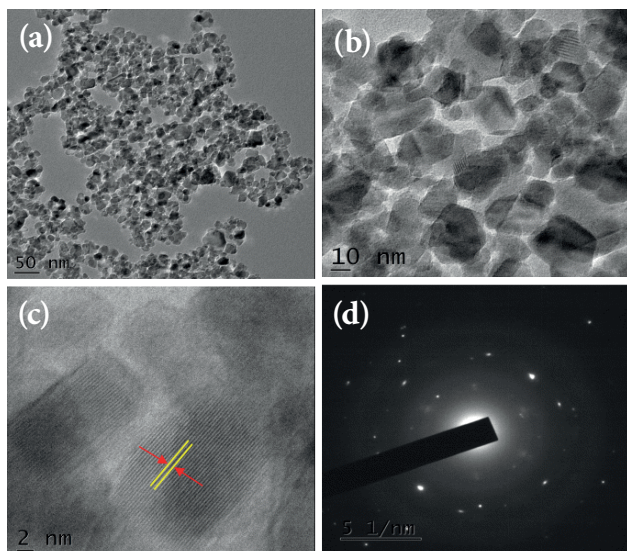


Fig. 3 HR- TEM images of the 9% wt *MMT/CdAl₂O₄* photocatalyst at (a) 50 nm, (b) 10 nm and (c) Lattice fringes at 2 nm and (d) SAED pattern on 5 1/nm

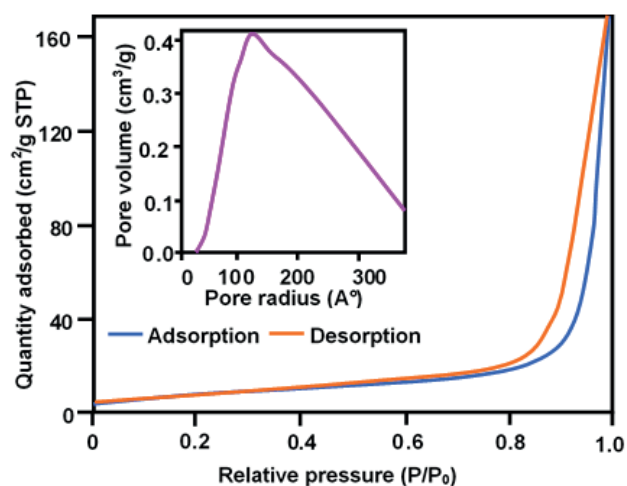


Fig. 4 BET adsorption-desorption isotherms and pore size distribution plots of the 9% wt *MMT/CdAl₂O₄* photocatalyst

The pore structure and surface area of 9% wt *MMT/CdAl₂O₄* photocatalyst were examined using nitrogen adsorption-desorption isotherms. The Barrett-Joyner-Halenda (BJH) technique was employed to analyze the pore size distribution. Notably, as shown in Figure 4, a significant enhancement in the adsorption volume of N₂ in the P/P₀ range of 0.65 to 0.90, indicating good homogeneity and macroporous size in the catalyst. In addition, the average pore radius, as indicated by the pore size distribution plot presented in the insert of Fig-

ure 4, is 125.7Å for the 9% wt *MMT/CdAl₂O₄* and bare CdAl₂O₄ has pore radius of 90.23Å. The resultant 9% wt *MMT/CdAl₂O₄* photocatalyst exhibits a large specific surface area of 42.15m²g⁻¹, compared to undoped CdAl₂O₄ (20.4m²g⁻¹) contributing to its improved photocatalytic activity.

To gain further insight into the photocatalytic mechanism, various factors, including optical absorption, emission properties, and specific area, were considered. An efficient material requires an appropriate band-gap to absorb light efficiently, generating charge carriers that catalyze the breakdown of dye molecules. In addition, the diffuse reflectance spectra of undoped CdAl₂O₄ and 9% wt *MMT/CdAl₂O₄* photocatalysts are shown in Figure 5a and 5b, respectively.

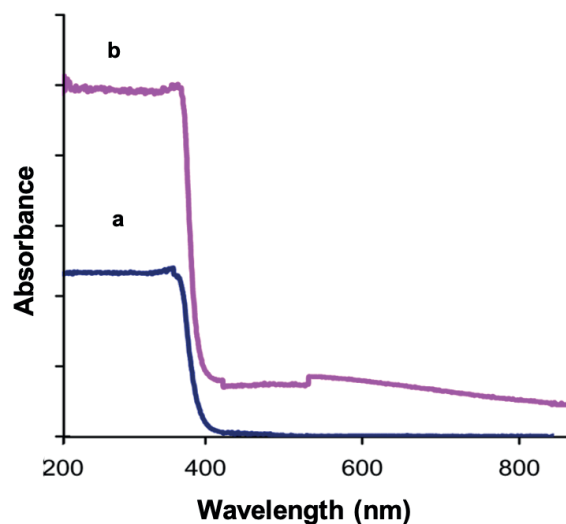


Fig. 5: Diffuse reflectance spectra of the (a) undoped CdAl₂O₄ and (b) 9% wt *MMT/CdAl₂O₄* photocatalysts

In the UV region, 9% wt *MMT/CdAl₂O₄* photocatalyst exhibits double the intensity of UV absorption compared to undoped CdAl₂O₄. The addition of 9% wt MMT results in a significant rise in the resultant peak intensities and a little decrease in E_g values. The energy gap of *MMT/CdAl₂O₄* nanoparticles is computed using the Tauc plot, which is afforded in the following equation

$$\alpha = A(h\nu - E_g)^{1/2} / h\nu$$

Where E_g, α, A and hν signify energy gap, photon energy, absorption coefficient, and the proportionality constant, The E_g of all synthesized materials were computed by linear fitting (αhν)² versus photon (hν) energy as 3.35 [30, 32] and 2.81eV for undoped CdAl₂O₄ and *MMT/CdAl₂O₄* nanoparticles respectively as displayed in Fig. SI.2

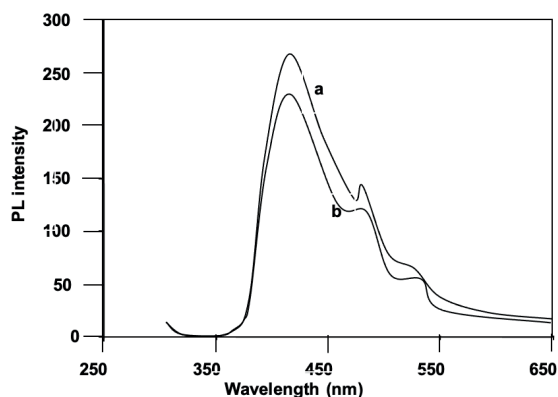


Fig. 6 Photoluminescence spectra of the (a) undoped CdAl₂O₄ and (b) 9% wt MMT/CdAl₂O₄ photocatalysts

In addition, Figure 6a and 6b display the photoluminescence spectra of undoped CdAl₂O₄ and 9% wt MMT/CdAl₂O₄ photocatalysts, respectively. The photoluminescence intensity of 9% wt MMT/CdAl₂O₄ photocatalyst is lower than that of undoped CdAl₂O₄, indicating reduced electron-hole pair recombination due to the presence of loaded MMT on CdAl₂O₄. This reduction in fluorescence intensity contributes to enhanced photocatalytic activity and reduced electron-hole pair recombination.

3.2. Photocatalytic Study

Figure 7 illustrates the photocatalytic activity of the synthesized undoped CdAl₂O₄, 5% wt MMT/CdAl₂O₄ and 9% wt MMT/CdAl₂O₄ towards the removal of rh-B dye by direct solar-light radiation. The dye is resistant to self photolysis and for the same experiment with MMT/CdAl₂O₄ in the dark, a decrease (10%) in dye concentration was observed due to the adsorption of dye on the catalyst. The degradation outcomes display there is no significant changes in dye concentration under the absence of light and catalyst. With 9% wt MMT/CdAl₂O₄ photocatalyst, rh-B dye almost completely degrades within 45 minutes. However, under the same conditions, undoped CdAl₂O₄ and 5% MMT/CdAl₂O₄ achieved 68% and 78.5% degradation of rh-B dye, respectively. The montmorillonite clay shows nearly 35% of adsorption. These results indicate that the prepared 5% MMT/CdAl₂O₄ photocatalyst is more effective than other catalysts in degrading rh-B when exposed to direct solar-light. This underscores higher photocatalytic activity of MMT/CdAl₂O₄ photocatalyst, attributed to the loaded MMT clay. Under UV light irradiation MMT/CdAl₂O₄ produce maximum dye degradation percentage compare other pure MMT clay and undoped CdAl₂O₄ (Fig. SI.4).

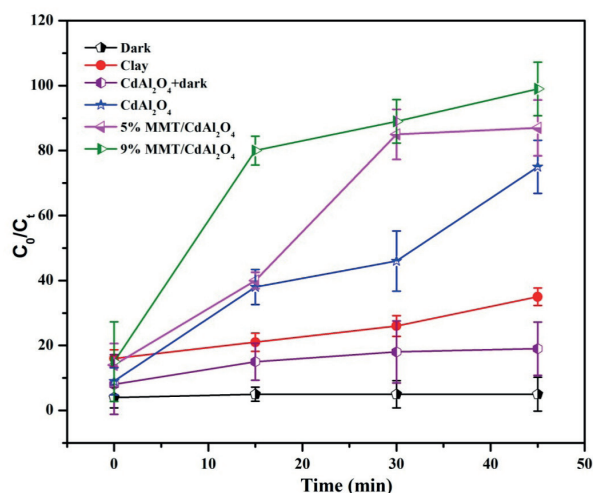


Fig. 7 Photodegradation of rh-B dye with different catalysts: dye concentration = 3×10^{-4} M, catalyst suspended = 3 g L^{-1} , pH = 7, airflow rate = 8.1 mL s^{-1} , $I_{\text{solar}} = 1250 \times 100 \text{ Lux} \pm 10$. Irradiation time = 45 min)

Under visible irradiation, the e^- on MMT doped CdAl₂O₄ sample are photoexcited into their particular (CB), leaving h^+ on the valence band (VB), thereby making photoexcited charge carriers. The photoexcited e^- on the CB of MMT doped CdAl₂O₄ rapidly transformed into that of trapping level of MMT/CdAl₂O₄, while the photoexcited h^+ on the VB of MMT/CdAl₂O₄ reacts with the water molecules to produce the OH radicals and generated e^- near to CB of the trap state can interact with the dissolved O₂ to produce O₂⁻ (superoxide radicals). Finally, these two radicals O₂⁻ and OH react with the dye molecule and convert the dye into CO₂ and H₂O. Further, the increased degradation efficiency can be attributed to two primary factors such as (i) MMT's ability to absorb UV light, doubling the absorption compared to undoped CdAl₂O₄ and (ii) the larger surface area of MMT/CdAl₂O₄ photocatalyst compared to undoped CdAl₂O₄ photocatalyst. In fact, MMT is an electron acceptor due to the presence of Lewis acids. The electrons from these aluminum sites are then transferred to the O₂ molecules in the CdAl₂O₄ solution, which result in delay in the recombination reaction. Additionally, the presence of metal oxides in loaded MMT contributes to this electron transfer and may lead to the formation of sporadic energy levels, reducing the band gap energy and preventing electron-hole recombination [34]. A proposed mechanism in Figure 8 views MMT as an impurity in the attached with CdAl₂O₄ photocatalyst.

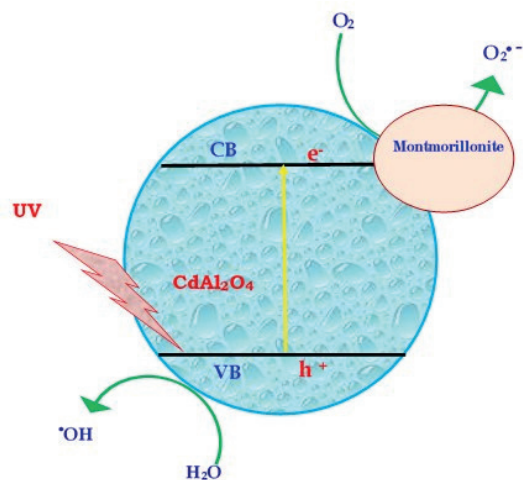


Fig. 8 A possible photodegradation mechanism of the *MMT/CdAl₂O₄* photocatalyst

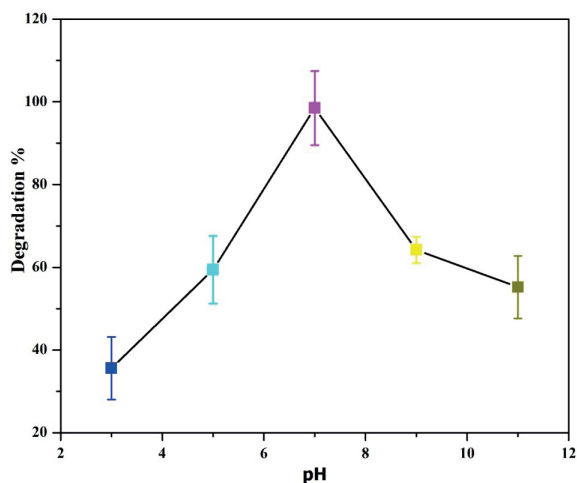


Fig. 9 Effect of solution pH on rh-B degradation using 9% wt *MMT/CdAl₂O₄* photocatalyst (dye concentration = 3×10^{-4} M, catalyst suspended = 3 gL^{-1} , airflow rate = 8.1 mLs^{-1} , $I_{\text{solar}} = 1250 \times 100 \text{ Lux} \pm 10$, irradiation time = 45 min)

The pH of the solution significantly affects photocatalytic degradation. Figure 9 illustrates the impact of pH on the photocatalytic removal of rh-B within the pH range of 3–11. The results indicate that increasing the pH from 3 to 7 enhances rh-B removal ability, with a neutral pH of 7 being the optimal condition for effective rh-B removal using the 9% wt *MMT/CdAl₂O₄* photocatalyst.

To evaluate the reusability of the 9% wt *MMT/CdAl₂O₄* photocatalyst for photoreactions, the catalyst was removed and cleaned with methanol following the complete dye degradation. The recovered catalyst, after dry-

ing for 90 minutes at 100°C, was utilized in the subsequent cycle. Five consecutive cycles of rh-B degradation under solar light demonstrated the photocatalyst's good stability and reusability (Figure 10). Until the fourth cycle, there is a slight decrease in degradation; after that, no further change is observed. In the fourth run, at 45 minutes of radiation, a degradation efficiency of 95.5% was achieved. These findings demonstrate that 9% wt *MMT/CdAl₂O₄* photocatalyst exhibits excellent stability and reusability.

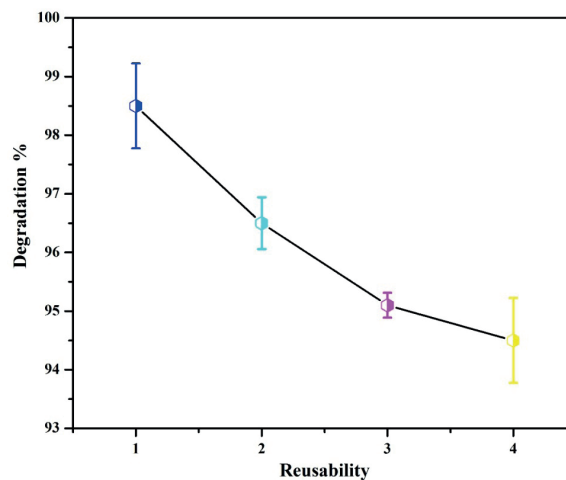


Fig. 10 Reusability of 9% wt *MMT/CdAl₂O₄* photocatalyst on rh-B degradation (dye concentration = 3×10^{-4} M, pH = 7, catalyst suspended = 3 gL^{-1} , airflow rate = 8.1 mLs^{-1} , $I_{\text{solar}} = 1250 \times 100 \text{ Lux} \pm 10$, irradiation time = 45 min)

3.3 Hydrophobicity property

Water-repellent materials find a wide range of applications, and this property was studied using water contact angle assessments (Figure 11). The contact angle of an uncoated glass slide is 37.2° (Figure 11a), which increases progressively with increasing TEOS values (58.4° , Figure 11b), TEOS + CdAl₂O₄ (80.5° , Figure 11c), TEOS + 5% wt *MMT/CdAl₂O₄* (100.2° , Figure 11d), and TEOS + 9% wt *MMT/CdAl₂O₄* (113.8° , Figure 11e). The extreme hydrophobicity properties of TEOS (Tetraethyl orthosilicate)-containing *MMT/CdAl₂O₄* is evident, with the O-Si-O groups being altered and the surface becoming rougher due to the presence of 9% wt MMT with CdAl₂O₄. In general, the catalyst's hydrophobic nature results in water contact angle of 90° [35]. This hydrophobic nature results in a water contact angle of 113.8° , further demonstrating its extreme hydrophobicity property.

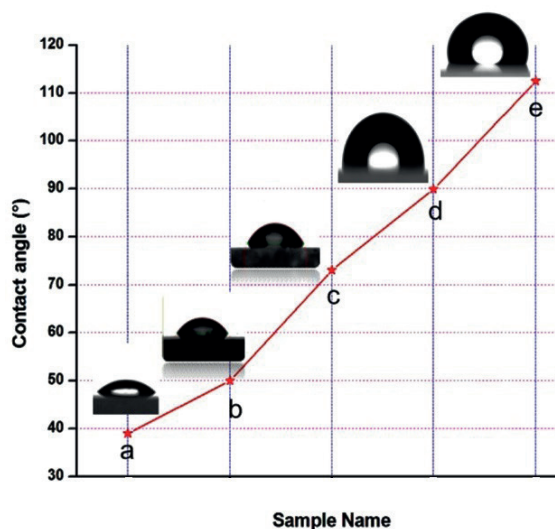


Fig. 11 Water contact angle assessments (a) uncoated glass slide, (b) TEOS coated glass slide, (c) TEOS+CdAl₂O₄ and (d) TEOS+5% wt MMT/CdAl₂O₄ and (e) TEOS/9% wt MMT/CdAl₂O₄

4. CONCLUSIONS

In summary, a facile hydrothermal co-precipitation technique was employed to produce montmorillonite-supported CdAl₂O₄ (MMT/CdAl₂O₄) without using any surfactants or organic solvents. The FE-SEM results showed that the as synthesized photocatalyst consists of microflakes and nanoclusters structures. The HR-TEM results confirmed the homogeneous spreading of elements, indicating the strongly attached within oxides, where particles take on hexagonal and spherical structures. Photodegradation results reveal that 9% MMT-supported CdAl₂O₄ is much effective at degrading rh-B dye than both raw and undoped CdAl₂O₄, particularly at neutral pH 7. Reduced fluorescence intensity in MMT/CdAl₂O₄ leads to decreased electron-hole pair recombination and improved photocatalytic activity. Moreover, the montmorillonite/CdAl₂O₄ showed a water contact angle of 113.8°, showing its extreme hydrophobic nature. This study introduces a novel application for montmorillonite, naturally occurring clay, in semiconductor oxide materials for energy and environmental applications.

ACKNOWLEDGEMENT

The authors express their gratitude to the Kalaig-nar Karunanidhi Government Arts College's principal

and the head of the chemistry department for providing a space for conducting research and for their continued support.

SUPPLEMENTARY INFORMATION

To learn more about the characterization data of montmorillonite supported CdAl₂O₄ nanocomposites, refer to the supplementary information file, which contains XRD pattern of 9% wt Montmorillonite clay supported CdAl₂O₄, Tauc energy plot, EDAX image of Montmorillonite clay and Photodegradability of Rh-B dye with different catalysts.

DECLARATIONS

Ethical Approval

Not applicable

Competing interests

There was no indication of potential conflicts of interest by the authors.

Authors' contributions

The data was collected by K. Kalpana

The data analysis was done by Dr. K. Rajathi.

Funding

Not applicable

Availability of data and materials

The writers are unwilling to share the data they used.

REFERENCES

1. S. Boudiaf, N. Nasrallah, M. Mellal, C. Belabed, B. Belhamdi, D. Meziani, M. Trari, *Optik* **2020**, *219*, 165038.
2. G. Wu, W. Wang, L. Cai, Y. Hong, Y. Jiang, C. Wang, *React. Kinet. Mech. Cat.* **2016**, *119*, 523-535.
3. J. Li, S. Wang, G. Sun, H. Gao, X. Yu, S. Tang, Y. Wei, *Mater. Today Chem.* **2021**, *19*, 100390.
4. X. D. Hou, X. Q. Guan, Y. F. Cao, Z. M. Weng, Q. Hu, H. B. Liu, J. Hou, *Int. J. Biol. Macromol.* **2020**, *145*, 620.
5. G. Panthi, O. H. Kwon, Y. S. Kuk, K. R. Gyawali, Y. W. Park, M. Park, *Catalysts* **2020**, *10*, 348.

6. H. Fan, X. Zhao, J. Yang, X. Shan, L. Yang, Y. Zhang, *Catal. Commun.* **2012**, 29, 29-33.
7. M. Bahrami, A. Nezamzadeh Ejjieh, *Mater. Sci. Semicond. Process* **2015**, 30, 275-284.
8. K. Thirumalai, S. Balachandran, M. Swaminathan, *Materials Chemistry and Physics* **2016**, 183, 191-200.
9. N. Nadeem, M. Zahid, Z. A. Rehan, M. A. Hanif, M. Yaseen, *International Journal of Environmental Science and Technology* **2021**, 19, 3045-3060.
10. K. Thirumalai, E. T. Deva Kumar, R. Aravindhana, J. Raghava Rao, and M. Swaminathan, *Surfaces and Interfaces* **2016**, 5, 30-38.
11. G. K. Zhang, X. M. Ding, F. S. He, X. Y. Yu, J. Zhou, Y. J. Hu, J. W. Xie, *Langmuir* **2008**, 24 (3), 1026-1030.
12. M. Mylarappa, N. Raghavendra, N. R. Bhumika, C. H. Chaithra, B. N. Nagalaxmi, K. N. Shrivana Kumara, *Chem.Phys.Mater.* **2023**, 3, 83-93.
13. M. Mylarappa, N. Raghavendra, B. S. Surendra, K. N. Shrivana Kumar, S. Kantharaju, *Applied Surface Science Advances* **2022**, 10, 100268.
14. M. Mylarappa, S. Chandruvasan, B. Thippeswamy, K. N. Shrivana Kumara, S. Kantharaju, *Sustainable Chemistry for the Environment* **2023**, 2, 100007.
15. F. Uddin, *j. intech. open* **2018**, 77987.
16. H. Liang, Z. Wang, L. M. Liao, L. Chen, Z. Li, J. Feng, *Optics*. **2017**, 136, 44-51.
17. I. Fatimah, T Huda, *Applied Clay Science* **2013**, 74, 115-120.
18. N. Yaghmaeiyan, M. Mirzaei, R. Delghavi, *Results in Chemistry* **2022**, 4, 100549.
19. K. G. Bhattacharyya, S.S. Gupta, *Adv. Colloid Interface Sci.* **2008**, 140, 114.
20. K. Fuminao, W. Toru, and O. Tatsuya, *ACS Appl Mater Interfaces*. **2020**, 12(6), 7021-7029.
21. Karthika, V. Srivastava, *E3S Web of Conferences* **2023**, 453, 01058.
22. P.R. Ashok, S. Grigorly, B. Subhash, *Current Pharmaceutical Biotechnology* **2021**, 22(6), 773-792.
23. A. Bouhemadou, F. Zerarga, A. Almuhayya, S. Bin-Omran, *Mater. Res. Bull.* **2011**, 46 (12), 2252-2260.
24. L. K. Kurihara, S. L. Suib, *Chem. Mater* **1993**, 5(5), 609-613.
25. A. Manzar, G. Murtaza, R. Khenata, M. Yousaf, S. Muhammad, Hayatullah, *Chin. Phys. Lett.* **2014**, 31(6), 67401-67404.
26. Z. Lv, Q. Chen, Y. Guo, *Solid State Sciences* **2020**, 109, 106393.
27. R. Kumar, M. A. Barakat, B. A. Al Mur, F. A. Alserury, J. O. Eniola, *J. Clean. Prod.* **2020**, 246, 119076.
28. Y. Ma, W. Ran, *J. Alloys Compd.* **2020**, 842, 155787.
29. G. Rajesh, P. Senthil Kumar, R. Gayathri, S. Akilandeswari, Mandal, A. Aindrila, V. Uma Shankar, M. Ramya, K. Nirmala, K. Thirumalai, *Mol. Catal.* **2023**, 535, 112835.
30. A. Rafiq, M. Ikram, S. Ali, F. Niaz, M. Khan, Q. Khan, M. Maqbool, *Journal of Industrial and Engineering Chemistry* **2021**, 97, 111-128,
31. W. Ran, L. Wang, Q. Liu, G. Liu, D. Qu, X. Pan, J. Shi, *RSC Adv.* **2017**, 7, 17612.
32. P. Rajesh, P. Senthil Kumar, S. Akilandeswari, G. Rangasamy, S. Lohita, V. Uma Shankar, M. Ramya, K. Thirumalai, *Chemosphere* **2023**, 32, 138232.
33. T. Watanabe, T. Sato, *Clay Sci.* **1988**, 7, 129-138.
34. S. Mahalaxmi, G. Rajesha, P. Senthil Kumara, S. Akilandeswari, M. Arul Joshua, V. Uma Shankar, M. Ramya, K. Thirumalai, R. Gayathri, *Chemosphere* **2023**, 322, 138178.
35. V. Maja, L. Mika, L. Kai, H. Tommi, H. A. R. Ras, *Soft Matter* **2019**, 15, 7096.

